Microearthquake Fracture Properties and Fluid-Driven Lubrication Processes Along a Complex Normal Fault System in Southern Apennines, Italy

http://www.rissclab.unina.it

Istituto Nazionale di Geofisica e Vulcanologia

Antonella Orefice (1), Aldo Zollo (1) and Vincenzo Convertito (2)

(1) Dept. of Physics, University Federico II, Naples, Italy; (2) Istituto Nazionale di Geofisica e Vulcanologia - Osservatorio Vesuviano, Napoli, Italy

orefice@na.infn.it

EGU2013-10588

European Geosciences Union General Assembly 2013

1. Abstract

We analyzed the P- and S-wave displacement spectra of 700 microearthquakes in the moment range $4x10^9$ - $2x10^{14}$ Nm and recorded at the dense, wide-dynamic range, seismic networks (Irpinia Seismic Network, ISNet, and Istituto Nazionale di Geofisica e Vulcanologia, INGV) operating in southern Apennines (Italy). Source parameters are estimated by a parametric modeling approach which is combined with a multi-step, non-linear inversion strategy. Estimates of the attenuation parameter t*=T/Q are obtained from the spectral decay of small earthquakes below the corner frequency and from the inversion of displacement spectra of relatively larger magnitude events. A Qs/Qp greater than 1 is found in the same depth range where high Vp/Vs and a peak in seismicity distribution are observed. This is the evidence for a highly fractured, partially fluid-saturated medium embedding the Irpinia fault zone, down to crustal depths of 15-20 km.

A nearly constant stress drop (8.3 MPa) and apparent stress (3.1 MPa) scaling of P- and S-corner frequencies and seismic energies is observed above a seismic moment value of about 10^{11} Nm.

The ratio between apparent stress and static stress drop (Savage-Wood seismic efficiency) is relatively high (0.5), indicating that the radiated energy is a very large fraction of the sum of energies spent by friction and fracture development. Seismic efficiency appears to be higher in the same depth range where high Vp/Vs and Qs/Qp values are also observed. This suggests that dynamic weakening driven by crustal fluid pressurization is the most plausible mechanism controlling the seismic radiation from microearthquake ruptures along the studied fault zone.

2. Seismic network, data acquisition and processing

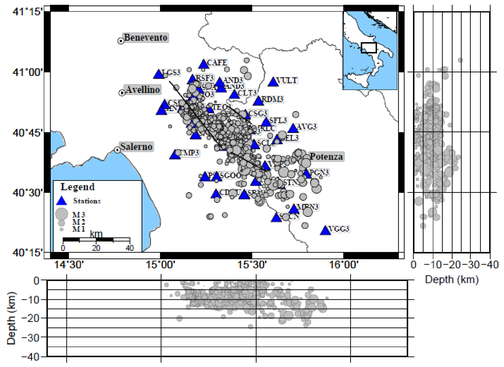

Map showing the microearthquakes analyzed in this study (grey circles) and stations of ISNet and INGV networks (solid triangles). Events are plotted with a symbol whose size is proportional to the magnitude. The three main rupture fault segments of the M_S 6.9 , 1980 Irpinia earthquake are also drawn as from Bernard and Zollo (1989).

Flow chart of pre-selection of data.
The earthquake locations have been computed using the NLLoc code (Lomax et al., 2000) and the minimum 1D P- and S-wave velocity models, as obtained by Matrullo et al. (2013) from the inversion of the first arrival times using VELEST code (Kissling et al., 1994).

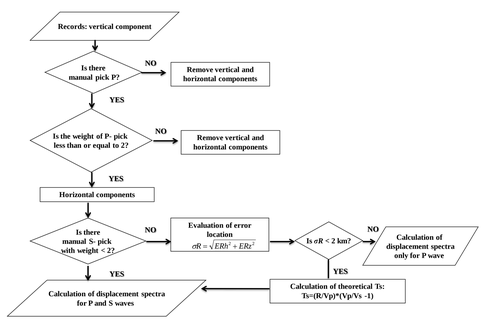

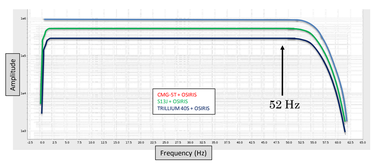

For the spectral analysis, we have chosen magnitude dependent frequency band limits, by extending it at higher frequencies for the analysis of the smallest events in the sequence. By taking into account the overall instrument response curves for ISNet and INGV stations, which include the data-logger and sensor responses, we determined the whole usable frequency bandwidth to be 0.4 – 50 Hz. Within this frequency band, the recorded signals have been preliminarily corrected for the overall instrument response curves, considering for each station its specific seismic sensor type and data-logger transfer function.

3. Iterative, multi-step inversion of P and S displacement spectra

Spectral model

The observed displacement spectrum U can be described by the relationship:

$$U(f) = C_s \frac{\Omega_0}{1+\left(\frac{f}{f_c}\right)^{\gamma}} \cdot \exp(-\pi t f) \cdot R(f)$$

- C_S is a constant that accounts for direct P- and S-wave amplification due to a vertically varying velocity structure
- Ω_0 is the low-frequency spectral level, f_c is the corner frequency, γ is the high-frequency spectral fall-off parameter, assumed here to vary in the range 1-3
- $t^*=T/Q$ is the attenuation parameter which depends on the travel time T and the quality factor Q
- R(f) is the site transfer function that is generally frequency dependent and accounts for site amplification/attenuation effects related to the local geology. As a first order approximation, in this study we assumed that R(f) = R_j (j is the station index), e.g. the site transfer function is constant in the whole considered frequency range.

Path attenuation model and estimation of the parameter t*

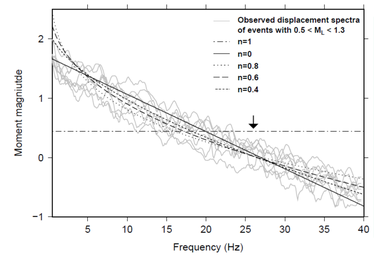

In the present study, the hypothesis of a frequency dependent-Q ($Q(f)=Q_0 \cdot f^n$) has been statistically tested versus the constant-Q model, based on the analysis of displacement spectra for low magnitude events (M_L < 1.5). Assuming a constant stress drop of 8 MPa (this values being inferred from the analysis of the larger magnitude events), and the Madariaga (1976) source model, the source spectrum of M_L<1.5 earthquakes becomes asymptotically constant for frequencies smaller than about 28 Hz and can be fitted for different n-values (see figure on the left).

The statistical test indicates that the Q-costant model provides the best compromise between model simplicity and adherence to data (Akaike, 1974).

Estimate of t* and Mo for small size (M_L≤1.5) earthquakes

For events with M_L≤1.5 the seismic moment and t* coefficient are obtained by a technique which measures the intercept and slope of the logarithm of the displacement spectrum at frequencies smaller than the expected corner frequency.

$$\log S_s(f < f_c) = \log S_o - \pi t f$$

The range of frequencies used to perform the analysis is 6-20 Hz. In order to obtain reliable estimates of both t* and So, the procedure has been applied only to those spectra characterized by a linear decreasing trend, e.g. showing a linear correlation coefficient CC ≤ -0.7.

Determination of source and attenuation parameters: iterative, multi-step inversion strategy

Flow chart of iterative, multi-step inversion strategy
An iterative, multi-step method has been applied to determine the source and attenuation parameters from the inversion of P- and S-wave displacement spectra of microearthquakes with M_L≥1.0. Steps 1 to 3 are iterated till no or negligible change in the average values of of $<\gamma^*_{ij}>$ and $<t^*_{ij}>$ are observed. Preliminary tests have confirmed that the convergence toward stable values of $<\gamma^*_{ij}>$ and $<t^*_{ij}>$ is reached only after 3-4 iterations.

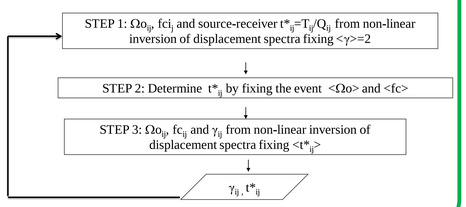

4. Results

P- and S- travel path attenuation and high-frequency spectral fall-off parameters

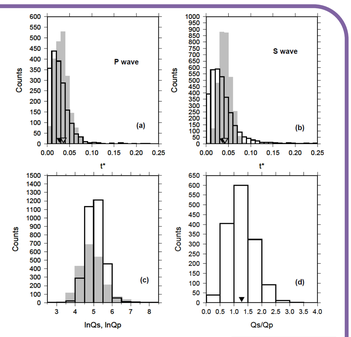

Distributions of the parameter t* for both P- (panel a) and S-waves (panel b) as obtained applying the iterative multi-step procedure (black) and the technique for smaller events (grey). The triangles represent the mean values of the t* parameter obtained from both the two methods. (Panel c) The log-normal distribution of parameters Q for P (grey) and S-waves (black). (Panel d) Distribution of Qs/Qp ratio. The average value (1.3 ± 0.5) is indicated with triangle.

We found that the mean values of γ for P- and S- wave are comparable within the errors, i.e. γ_P = 1.88 ± 0.55 and γ_S = 1.80 ± 0.53. These values are close, but systematically smaller than those expected for an ω^{-2} spectral model.

P- and S- site term

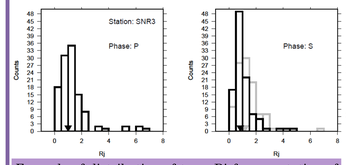

Example of distribution of term Rj for one station of ISNet network. For P-wave it is obtained analyzing the signals recorded by velocity sensors, while for S-wave by velocity (black) and accelerometer (grey) sensors. In each panel the triangles represent the median value of Rj.

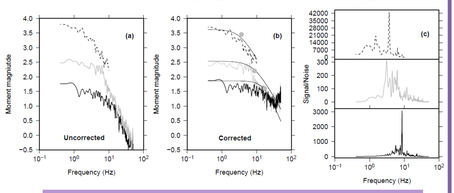

The comparison between corrected and uncorrected displacement spectra (panels a and b in figure on the left) demonstrates the effectiveness of the static site terms/factors.

Seismic moment, source radius and static stress drop estimates

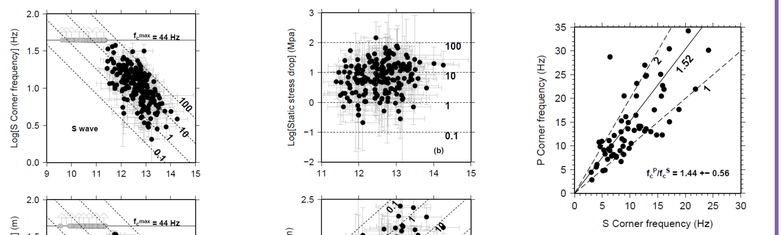

Measured seismic moments and corner frequencies for P-wave (bottom panel) and S-wave (upper panel) .Dashed lines refer to constant stress-drop values expressed in MPa. Solid lines mark the maximum resolution corner frequency set at 44 Hz. The corner frequencies greater then 44 Hz are plotted at the limit with upward arrows.

Panel a: Log of the measured Madariaga (1976)' source radius model as function of the log of the seismic moment.
Panel b: Log of static stress drop as function of the log of the seismic moment.

P-wave and S-wave measured corner frequencies for a limited portion of the analyzed dataset.
Dashed lines show different P/S corner frequencies ratio.
The data suggest $f_c^P/f_c^S \approx 1.5$.

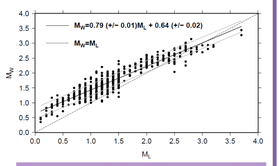

Moment magnitude (M_W) versus local magnitude (M_L) relationship obtained from a best fit analysis.

P- and S-wave seismic energies and apparent stress estimates

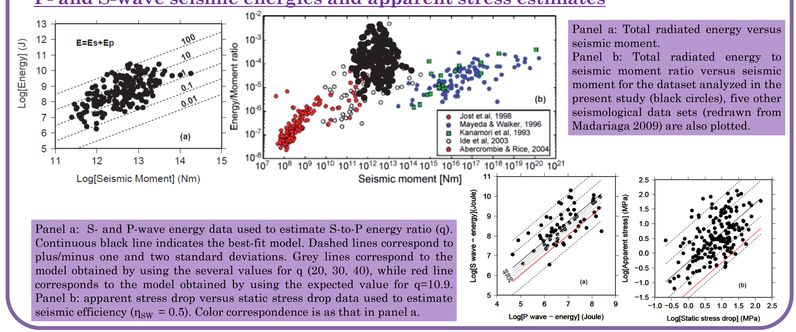

Panel a: S- and P-wave energy data used to estimate S-to-P energy ratio (q). Continuous black line indicates the best-fit model. Dashed lines correspond to plus/minus one and two standard deviations. Grey lines correspond to the model obtained by using the several values for q (20, 30, 40), while red line corresponds to the model obtained by using the expected value for q=10:9.
Panel b: apparent stress drop versus static stress drop data used to estimate seismic efficiency (η_{SW} = 0.5). Color correspondence is as that in panel a.

Panel a: Total radiated energy versus seismic moment.
Panel b: Total radiated energy to seismic moment ratio versus seismic moment for the dataset analyzed in the present study (black circles), five other seismological data sets (redrawn from Madariaga 2009) are also plotted.

5. Conclusions

1. We analyzed and modeled the displacement spectra of about 717 microearthquakes in the moment range $4x10^9$- $2x10^{14}$ Nm (M_W 0.3 – 3.5) and rupture sizes between few tens to few hundreds of meters, occurring along the normal fault system of the southern Apenninic belt.
2. Statistical tests confirm that the constant-Q model both for P- and S-waves in the analyzed frequency range (0.4-50 Hz) has to be preferred to frequency dependent Q-models for modeling the path attenuation effect in the investigated area. We estimate a crustal Q_S higher than Q_P and a greater than 1 in the same depth range where high Vp/Vs and a peak in seismicity distribution are observed. This is an evidence for a highly fractured, partially fluid-saturated medium embedding the Irpinia fault zone, down to crustal depths of 15-20 km.
3. A nearly constant stress drop (8.3 MPa) and apparent stress (3.1 MPa) scaling of P- and S-corner frequencies and seismic energies is observed down to a seismic moment value of about 10^{11} Nm and a Madariaga' source radius of 50 m. The observed ratios between P- and S-corner frequencies ($f_c^P/f_c^S \approx 1.5$) is consistent with the values expected from theory, while the S- and P-radiated energies ratio ($E_S/E_P \approx 55$) is higher than predicted value (11).
4. The ratio apparent to stress drop ratio (Savage-Wood seismic efficiency) is relatively high (η_{SW} = 0.5), indicating that radiated energy is a very large fraction of the sum of energies spent by friction and fracture development. It remains approximately constant over about four orders of magnitude, which is an evidence for apparent stress and static stress drop co-varying, independently on the fracture size, at least in the explored magnitude range.
5. Our results suggest that dynamic undershoot is the dominant mechanism controlling the seismic radiation from microearthquake ruptures along the Irpinia fault zone. It is consistent with the hypothesis of a dominant weakening effect driven by pressurization of fluids which saturate a densely fractured and porous crustal volume confined within the Irpinia fault system.

References

Akaike, H. (1974), A new look at the statistical model identification, IEEE Trans. Autom. Control, 6, 716–723.

Bernard P. and A. Zollo (1989) The Irpinia (Italy) 1980 earthquake: detailed analysis of a complex normal fault, J. Geophys. Res., 94, 1631-1648.

Kissling E., Ellworth W.L., Eberhart-Phillips D. and Kradolfer U. (1994), Initial reference models in local earthquake tomography. J. Geophys. Res., 99, 19635–19646.

Lomax, A., J. Virieux, P. Volant, and C. Berge (2000), Probabilistic earthquake location in 3D and layered models: Introduction of a Metropolis-Gibbs method and comparison with linear locations, in Advances in Seismic Event Location, Thurber, C.H., and N. Rabinowitz (eds.), Kluwer, Amsterdam, 101-134.

Madariaga, R., (1976), Dynamics of an expanding circular fault, Bull. Seismol. Soc. Am., 66, 639-666.

Madariaga, R. (2009), Earthquake scaling laws, in Encyclopedia of Complexity and Systems Science, R. A. Meyers ed., Part 5, 2581-2600, Springer, New York, DOI: 10.1007/978-0-387-30440-3_156.

Matrullo, E., Amoroso O., De Matteis R., Satriano C. and A. Zollo, (2011) 1D versus 3D velocity models for earthquake locations: a case study in Campania-Lucania region (Southern Italy), Geophysical Research Abstracts Vol. 13, EGU2011-9305, 2011.

Acknowledgements

This work was financially supported by Dipartimento della Protezione Civile (DPC) and the Istituto Nazionale di Geofisica e Vulcanologia (INGV) within the research framework programs S5 and S3, and by EU-FP7 in the framework of project NERA.